Global-Synchronized Optimized Pulse Patterns

Guangze Chen, *Student Member, IEEE*, and Zhenbin Zhang, *Senior Member, IEEE*

***Abstract*—Optimized pulse pattern, a powerful technique to address harmonic issues for power converters at low switching frequencies, has been widely recognized in high power applications in both industry and academia. However, existing solutions primarily focus on the optimization of single converter scenarios. In this work, we propose a *global-synchronized optimized pulse pattern* technique for power converter clusters. As an upper-layer optimization strategy, the proposal utilizes the additional switching pattern freedom provided by the neighboring power converters and achieves extreme power quality at the common interface, even with ultra-low switching frequencies. Moreover, a pattern extension mechanism is designed to ensure sustained synchronization among units throughout the optimization interval, releasing the inherent computational challenge in the optimization problem. Experimental data confirm its effectiveness.**

***Index Terms*—Converter cluster, global-synchronized optimized pulse pattern (GS-OPP), harmonic distortion, programmed modulation.**

I. Introduction

Power converter-based energy conversion techniques have already been very aggressively adopted in modern power grids, electrification systems, energy storage, etc. In particular, as the power ratings of the modern power converter-dominated energy conversion system continue to grow, an increasing need to move beyond single-converter solutions and to develop techniques capable of effectively managing converter clusters has appeared.

Larger single-unit capacity offers higher energy capture efficiencies and lower costs per watt, thus recognized as a trend for the development of several renewable energies [1], particularly offshore wind energy generation. Currently, the largest capacity within a single wind turbine can be up to 26 MW (produced by DEC) in industrial settings, much higher than the previous predictions. To convey the substantial power efficiently while maintaining the thermal constraints, the power converter is commonly operated at a low switching frequency, typically several hundred hertz depending on specific power devices [2], e.g., gate turn-off thyristors (GTOs), integrated gate-commutated thyristors (IGCTs), insulated gate bipolar transistors (IGBTs). However, this leads to considerable distortion, polluting the grid and also increasing the filter costs.

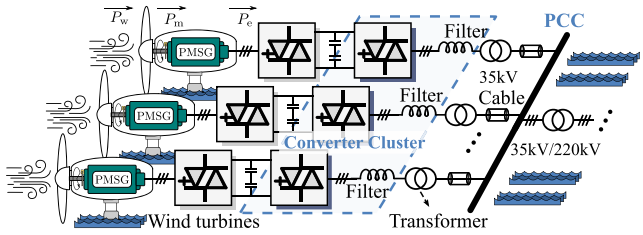

Fig. 1. Typical clustered case: offshore wind energy generation systems.

Pulsewidth modulation (PWM), linking the bridge of control and circuits, is a crucial part of power electronics that directly affects the harmonic distribution of the system. The techniques can be primarily categorized into three types, i.e., 1) carrier- [3], 2) space vector- [4], and 3) programmed-based modulation [5]. Among them, programmed-based modulation (PM), with its capability to directly manage harmonic characteristics, is highly competitive in high-power medium-voltage applications at low switching frequencies.

The history of PM can be traced back to the 1960s [6], with the usage of eliminations in several selected low-order harmonics. It is widespread and still competitive in high power applications in recent times [7], [8], [9]. However, the simple consideration on the complete elimination of finite selected orders leads to a local optimum in the total harmonic distortion (THD). To address such a problem, the PM with minimized THD is established [10]. Different from former techniques, the method solves an optimized harmonic distribution in the spectrum instead. Due to the flexible form of the optimization problem, such a technique has the capability to handle more complex and tailorable demands (e.g., common mode voltage [11], switching losses [12], thermal constraints [13]). In recent literature, these methods have been increasingly referred to under the unified terminology of optimized pulse patterns (OPPs) [11], [12], [13], [14] or synchronous optimal pulse width modulation (SOPWM) [24] , which offer effective solutions to harmonic issues under low switching frequency conditions. However, existing research predominantly focuses on individual converter systems. The potential of freedom given by converter clusters is seldom explored.

Clustered distribution of converters has become a promising trend in renewable energy plants, as it offers desirable stable power delivery, high reliability, and reduced maintenance costs. A typical offshore wind energy conversion cluster is shown in Fig. 1. The system consists of wind power units interconnected

Received 12 April 2025; revised 10 August 2025; accepted 30 September 2025. Date of publication 2 October 2025; date of current version 13 November 2025. This work was supported in part by the National Key R&D Program of China under Grant 2022YFB4201700, in part by the National Natural Science Foundation of China under Grant 52277191, in part by the National Natural Science Foundation of China under Grant 52277192, and in part by Science Fund for Distinguished Young Scholars of Shandong Province under Grant ZR2023JQ020. Recommended for publication by Associate Editor Y. A.-R. I. Mohamed. *(Corresponding author: Zhenbin Zhang.)*

The authors are with the School of Electrical Engineering, Shandong University, Jinan, Shandong 250061, China (e-mail: guangze.chen@mail.sdu.edu.cn; zbz@sdu.edu.cn).

Color versions of one or more figures in this article are available at https://doi.org/10.1109/TPEL.2025.3617250.

Digital Object Identifier 10.1109/TPEL.2025.3617250

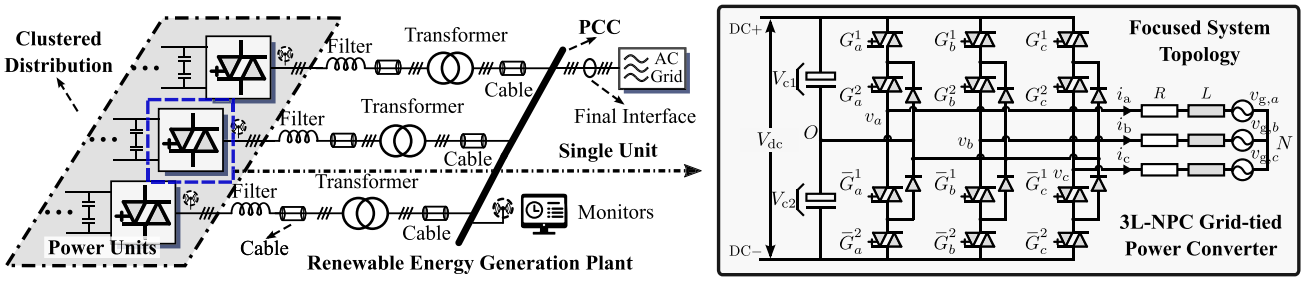

Fig. 2. High-power medium-voltage renewable energy generation plants and the structure of the 3L-NPC power converter.

to a point of common coupling (PCC), which then feeds power to the grid through a centralized substation. Since the final output interface of the plant is the PCC, harmonic optimization at the PCC is the ultimate goal. Xu and Gao [15] established a carrier-based global synchronous pulsewidth modulation (GS-PWM). The method adjusts the phase shift of carrier signals between different converters using a unified central computational unit, thereby achieving harmonic cancellation between the converters. This approach has demonstrated significant potential in photovoltaic systems with high switching frequencies and offers a valuable reference for coordinated modulation in converter clusters. However, its improvement is constrained in high-power systems, where limited switching frequency poses significant challenges to classical carrier-based schemes, and harmonic issues become more severe (see Section V).

In this work, we propose a global-synchronized OPP (GS-OPP) technique for the applications of converter clusters with limited switching frequencies. Through analyzing the harmonic characteristics within the converter clusters, a global optimization problem is formulated to obtain the optimized pulse sequence of each power unit. Its deployment is highly flexible and can be extended to any converter-based system having a common coupling point. Experimental data confirm its effectiveness and superiority. Major contributions include the following.

1) The coupling of harmonics and pulses within the cluster has been thoroughly analyzed (see Section III and Section IV).
2) A GS-OPP is proposed, achieving extreme power quality enhancement at the grid interface (see Section IV).
3) Case implementations have been experimentally demonstrated in the laboratory and benchmarked against several classical modulation techniques (see Section V).

The rest of this article is organized as follows. Section II introduces the system of converter clusters and the structure of a three-level neutral-point-clamped (3L-NPC) converter. Section III revisits the technique of harmonic programmed modulation. Section IV introduces the proposed GS-OPP. Section V illustrates the experimental results under the lab-constructed test bench. Finally, Section VI concludes this article.

II. System Description and Modeling

In this section, the system of power converter clusters is discussed, and the structure of a 3L-NPC power converter is introduced.

A. System Description

As depicted in Fig. 2, to facilitate management and reduce operational costs, power converters within a renewable energy generation plant are typically deployed in a clustered configuration. Each power unit is interconnected via transmission lines to a common ac bus[1] (i.e., PCC), where the aggregated power is then delivered to the main grid through a unified grid-connection interface. It is evident that, since the final grid-connection interface of the converter cluster is the PCC, enhancing the performance at the PCC becomes the most critical objective. This work specifically focuses on minimizing harmonic current injection in converter clusters under ultra-low switching frequencies, which is a typical constraint in high-power medium-voltage applications.

B. 3L-NPC Power Converter

3L-NPC power converter, due to its comprehensive performance of both the construction cost and power quality, is a competitive solution for high-power medium-voltage energy conversion. It has been widely adopted in various industrial products, e.g., ACS6080 produced by ABB [16], 3300 V full-power converter by Hopewind [17], etc. Thus, it is selected as a case study in this work.

As depicted in Fig. 2, the power circuit consists of four IGCTs in each converter arm, allowing for the generation of three possible voltage levels in a single phase. Here, we define the switching state u_x in phase x as

$$u_x := \mathcal{G}(G_x^i) = \begin{cases} 1, & \text{if } G_x^1 = 1 \ \& \ G_x^2 = 1 \\ 0, & \text{if } G_x^1 = 0 \ \& \ G_x^2 = 1 \\ -1, & \text{if } G_x^1 = 0 \ \& \ G_x^2 = 0 \end{cases} \quad (1)$$

where $x \in \{a, b, c\}$ denotes the phase of the power converter, G_x^i is the gate signal for upper IGCTs, and $i \in \{1, 2\}$ is the index of the gate signal as defined in Fig. 2. $\bar{G}_x^i$ is the gate drive signal for lower IGCTs (complementary to G_x^i).

Defining the dc-link capacitor voltages as V_{c1} and V_{c2}, the output arm voltage of the converter v_x (with respect to the converter's neutral point) is given by

$$v_x = \frac{V_{c1} + V_{c2}}{2} u_x - \frac{V_{c1} - V_{c2}}{2} |u_x|. \quad (2)$$

[1] Multiple common ac buses may also exist within specific renewable energy plants

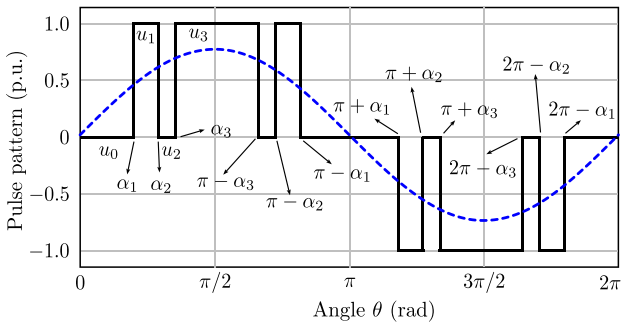

Fig. 3. Single-phase switching signal $u(\theta)$ with QaHWS, pulse number $d = 3$.

Assuming the dc-link voltage is $V_{\rm dc}$ and the clamping capacitor voltages are balanced (i.e., $V_{\rm c1} = V_{\rm c2}$), the arm voltage can be simplified as

$$v_x = \frac{V_{\rm dc}}{2} u_x. \tag{3}$$

III. Harmonic Programmed Modulation

In this section, the fundamental principles and design process of harmonic programmed modulation are reviewed, with a particular focus on classical POO. Hereafter, a representative set of three-level switching signals is selected as a case study for further demonstration.

In the following, the switching frequency of the semiconductor switches is defined as

$$f_{\rm sw} = d f_1 \tag{4}$$

where d is the number of the pulse and f_1 is the fundamental frequency of the switching signal. For example, the case shown in Fig. 3 corresponds to $d = 3$. That is, with a fundamental frequency of 50 Hz, the switching frequency is 150 Hz.

A. Pulse Patterns

Here, the definition of pulse pattern is first discussed. For programmed modulation, two assumptions are typically made to simplify calculations: 1) the switching signal is 2π-periodic. 2) the switching signal is three-phase symmetric. Thereby, the three-phase switching signals are fully characterized by the switching signal $u(\theta)$ in single-phase with the integer switching position $u \in \{-1, 0, 1\}$ and angle $\theta \in [0, 2\pi]$ [12]. In Fig. 3, a single-phase pulse pattern with quarter- and half-wave symmetry (QaHWS) is shown. The switching signal $u(\theta)$ of the first quarter period is fully defined by the switching angles α_i with $i \in \{1, 2, \ldots, d\}$. The rest is an extension of its quarter-cycle, i.e., $\alpha_{i+d} = \pi - \alpha_{d-i}$, $\alpha_{i+2d} = \pi + \alpha_i$, $\alpha_{i+3d} = 2\pi - \alpha_{d-i}$. Therefore, the pulse pattern can be expressed as

$$u(\theta) = \sum_{i=1}^{4d} \Delta u_i \mathcal{T}(\theta - \alpha_i). \tag{5}$$

Here, $\mathcal{T} \in \{0, 1\}$ is the step function, and Δu_i is the switching transition given as

$$\Delta u_i = u_i - u_{i-1},\ i \in \{1, 2, \ldots, d\} \tag{6}$$

which is defined as the change in switching position at the switching angle α_i. Due to only the nonnegative switch positions being considered in the first quarter cycle, the initial switching position u_0 is zero. Thereby, the switching transitions can be simplified as

$$\Delta u_i = (-1)^{i+1}. \tag{7}$$

B. Harmonics Decomposition

According to the Fourier series theory, any periodic signal that satisfies the Dirichlet conditions can be expanded into a series of sine/cosine functions of different frequencies, i.e.,

$$u(\theta) = \sum_{n=0}^{\infty} \left[a_n \cos(n\theta) + b_n \sin(n\theta)\right] \tag{8}$$

where n denotes the decomposed harmonic order, and a_n, b_n are the Fourier coefficients, which directly impact the amplitude $\hat{u}_n$ and phase ϕ_n of each order harmonic, i.e.,

$$\begin{cases} \hat{u}_n = \sqrt{a_n^2 + b_n^2} \\ \phi_n = \arctan(b_n / a_n). \end{cases} \tag{9}$$

Note that the amplitude of the fundamental component $\hat{u}_1$ is equal to the modulation index $\mathcal{M}$, with $\mathcal{M} \in [0, 4/\pi]$. The Fourier coefficients can be determined using the orthogonality of trigonometric functions.

For QaHWS switching signals, the coefficients can be expressed as

$$a_n = 0, \quad n = 0, 1, 2, 3, \cdots \tag{10a}$$

$$b_n = \begin{cases} \frac{4}{n\pi} \sum_{i=1}^{d} \Delta u_i \cos(n\alpha_i), & n = 1, 3, 5, \cdots \\ 0, & n = 0, 2, 4, \cdots \end{cases} \tag{10b}$$

With the symmetry characteristics, all harmonics of even order, the dc offset, and the Fourier coefficient a_n are zero. This simplifies the complexity of formulating subsequent solving problems. However, note that this will reduce the degree of freedom in exploring the power quality optimization problem, as the phase of the harmonics cannot be altered, i.e., $\phi_1 = \phi_n$.

For half-wave symmetry (HWS) switching signals, the coefficients can be expressed as

$$a_n = \begin{cases} -\frac{2}{n\pi} \sum_{i=1}^{2d} \Delta u_i \sin(n\alpha_i), & n = 1, 3, 5, \cdots \\ 0, & n = 0, 2, 4, \cdots \end{cases} \tag{11a}$$

$$b_n = \begin{cases} \frac{2}{n\pi} \sum_{i=1}^{2d} \Delta u_i \cos(n\alpha_i), & n = 1, 3, 5, \cdots \\ 0, & n = 0, 2, 4, \cdots \end{cases} \tag{11b}$$

Since both of a_n and b_n are tunable, the harmonic phases can be adjusted. However, at a cost, the complexity is increased.

C. Grid Currents

For voltage-source power converters, current is the primary variable for power interaction with the grid. Take the converter with L filters as an example, the simplified models can be expressed as Fig. 4. The grid currents can be expressed as

$$i = i_1 + i_{\rm h}, \tag{12}$$

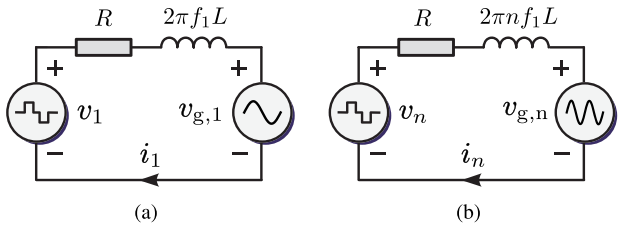

Fig. 4. Simplified models. (a) Fundamental model. (b) Harmonic model.

where $i_1 = \sqrt{2}I\sin(\theta + \phi^*)$ is the fundamental component. I is the rms value of the fundamental and ϕ^* is the displacement angle (typically a positive value, due to the inductive reactance characteristics of filters and transmission lines).

The second term in (12) is the harmonic components

$$i_{\mathrm{h}} = \sum_{n=5,7,11,\cdots}^{\infty} i_n \tag{13}$$

which is a lumped parameter representing the superposition of harmonic currents i_n in each order. Due to the three-phase symmetry of the system, triple harmonics will not be reflected in the current, thereby only $6k \pm 1$ orders are considered.

For a harmonic current i_n in the nth order, it will be impacted by several variables, including converter voltage harmonics v_n, circuit parameters (parasitic resistance R and inductance L of the filter), and background voltage harmonics $v_{\mathrm{g},n}$ in the power grid

$$i_n = \frac{v_n - v_{\mathrm{g},n}}{\hat{z}_n \angle \phi_{\mathrm{z},n}} \tag{14}$$

where $\hat{z}_n$ is the impedance magnitude under nth order harmonic, and $\angle\phi_{\mathrm{z},n}$ is the impedance angle, i.e.,

$$\begin{aligned} \hat{z}_n &= \sqrt{(2\pi n f_1 L)^2 + R^2} \\ \angle\phi_{\mathrm{z},n} &= \arctan(2\pi n f_1 L/R). \end{aligned} \tag{15}$$

Since classical harmonic programmed modulation is typically calculated offline, background harmonics are difficult to estimate. Moreover, compared to the ripple induced by low-frequency switching, background influences are generally not the primary concern in low-switching-frequency applications. As a result, conventional programmed modulation methods typically do not take the impact of background into harmonic analysis [11], [12], [13], [14]. Therefore, the amplitude of the harmonic current $\hat{i}_n$ can be simplified as

$$\hat{i}_n = \frac{\hat{v}_n}{\sqrt{(2\pi n f_1 L)^2 + R^2}} \tag{16}$$

where $\hat{v}_n$ is the amplitude of the nth order voltage harmonic of the power converter

$$\hat{v}_n = \frac{V_{\mathrm{dc}}}{2}\hat{u}_n. \tag{17}$$

Due to the parasitic resistance being typically much smaller than the inductance, the complex of (16) can be further reduced

$$\hat{i}_{\mathrm{n}} = \frac{\hat{v}_n}{\sqrt{(2\pi n f_1 L)^2 + R^2}} \overset{R \ll 2\pi n f_1 L}{\approx} \frac{\hat{v}_n}{2\pi n f_1 L}. \tag{18}$$

D. Classical Optimized Pulse Patterns

Current harmonics cause additional losses in passive components and degrade power quality; thereby, it is desired to be minimized. THD is the most commonly used index to assess the quality of grid currents, which has been included in several grid standards [18]

$$I_{\mathrm{THD}} = \frac{\hat{i}_{\mathrm{h}}}{\hat{i}_1} = \frac{1}{\hat{i}_1}\sqrt{\sum_{n\neq 1}(\hat{i}_n)^2}. \tag{19}$$

Given that the fundamental current $\hat{i}_1$ remains constant under specific conditions, the optimization for THD can be proportional to

$$I_{\mathrm{THD}} \propto \sqrt{\sum\nolimits_{n=5,7,11,\cdots} \frac{1}{n^2}(\hat{u}_n)^2}. \tag{20}$$

Note that several excellent studies also refer to this form as the total demand distortion (TDD) [12], [13]. In essence, they are fundamentally equivalent

To obtain a set of pulse patterns that minimize the current THD under a fixed switching frequency, the following optimization problem can be formulated (QaHWS)

$$\min_{\alpha_i} \quad \frac{16}{\pi^2} \sum_{n=5,7,11,\ldots} \frac{1}{n^4}\left(\sum_{i=1}^{d} \Delta u_i \cos(n\alpha_i)\right)^2 \tag{21a}$$

$$\text{s.t.} \quad \frac{4}{\pi}\sum_{i=1}^{d} \Delta u_i \cos(\alpha_i) = \mathcal{M} \tag{21b}$$

$$0 < \alpha_1 < \alpha_1 \ldots < \alpha_d < \frac{\pi}{2}. \tag{21c}$$

Here, (21b) is designed to lead the fundamental voltage equal to the modulation index, and (21c) is to ensure the feasibility of the pulse sequence.

For a HWS pulse pattern, the optimization freedom of current harmonics is increased (harmonic phases); thus, the aforementioned problem is reformulated as

$$\min_{\alpha_i} \quad \sum_{n=5,7,11,\ldots} \frac{1}{n^2}(a_n^2 + b_n^2) \tag{22a}$$

$$\text{s.t.} \quad \frac{2}{\pi}\sum_{i=1}^{2d} \Delta u_i \cos(\alpha_i) = \mathcal{M} \tag{22b}$$

$$\frac{2}{\pi}\sum_{i=1}^{2d} \Delta u_i \sin(\alpha_i) = 0 \tag{22c}$$

$$0 < \alpha_1 < \alpha_2 \ldots < \alpha_{2d} < \pi \tag{22d}$$

where a_n and b_n is defined in (11). Note that the design of the optimized problem is flexible. Customization requirements

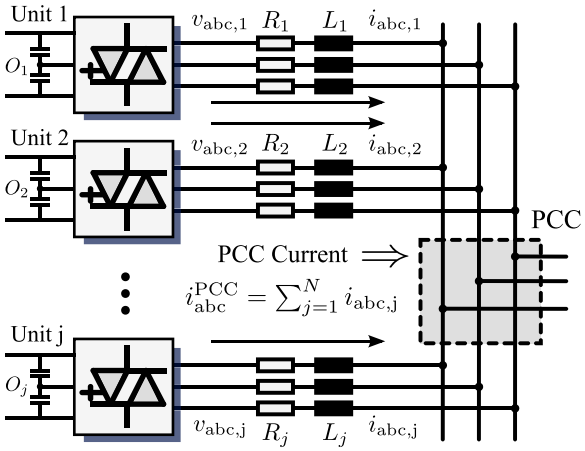

Fig. 5. Simplified model of a converter cluster with L filters.

can be explicitly embedded into the optimization problem (for further details, please refer to [19]).

OPPs offer an effective and powerful solution to harmonic issues arising from limited switching frequencies. [11], [12], [13]. However, the conventional theory is developed from the perspective of a single converter unit, leaving the additional degrees of freedom introduced by converter clusters unexplored. As a result, its optimization capability becomes limited in multiconverter coordinated scenarios (see Section V).

IV. Global-Synchronized Optimized Pulse Patterns

In the following sections, a GS-OPP is proposed to further utilize the additional switching combination freedom caused by the cooperation of multiple converters. Through deriving the harmonic model in the converter cluster and rebuilding the optimization problem, the THD in PCC current is significantly reduced. Furthermore, the tradeoff between PCC and single power converters is also discussed. Finally, a case implementation is introduced. Details are as follows.

A. PCC Optimization

A typical converter cluster is shown in Fig. 5. The individual converter currents merge at the PCC before being injected into the grid. Therefore, minimizing the current THD at the PCC is the desired objective of the system.

Assume the ac grid voltages v_{g} are three-phase balanced. Then, by Kirchhoff's law, the neutral point potential $v_{\mathrm{no},j}$ between the jth power converter and the grid is derived as

$$v_{no,j} = \frac{1}{3}(v_{a,j} + v_{b,j} + v_{c,j}) \tag{23}$$

where $v_{x,j}, x \in \{a,b,c\}$ is the jth converter voltage of phase x. Due to the three-phase symmetry of the switching signals, we select one phase for analysis. The currents of the jth power converter can be quantified as

$$i_{x,j} = \frac{1}{z_j}(v_{x,j} - v_{no,j} - v_{\mathrm{g},x}) \tag{24}$$

where z_j denotes the equivalent impedance of the L filter associated with the jth power converter. Due to the small parasitic resistance of the filter, z_j can be approximated as an inductance component $\hat{z}_j\angle 90$.

As derived in (10), a pulse sequence with QaHWS has a natural elimination in a_n, i.e., the fundamental and harmonics have the same phases. Therefore, the decomposed components of the three-phase sequence can be expressed as

$$\begin{cases} v_{a,n,j} = \hat{v}_{n,j}\sin(n\omega t), & n \in 1,3,5,\dots \\ v_{b,n,j} = \hat{v}_{n,j}\sin(n\omega t - \frac{2\pi n}{3}), & n \in 1,3,5,\dots \\ v_{c,n,j} = \hat{v}_{n,j}\sin(n\omega t + \frac{2\pi n}{3}), & n \in 1,3,5,\dots \end{cases} \tag{25}$$

where $\hat{v}_{n,j}$ is the amplitude of the nth order harmonic in jth power converter. Thereby, $v_{\mathrm{no},j}$ can be derived as

$$v_{\mathrm{no},j} = \frac{\hat{v}_{n,j}}{3}\left[\sin(n\omega t) + 2\sin(n\omega t)\cos\left(\frac{2\pi n}{3}\right)\right] \tag{26a}$$

$$= \begin{cases} \hat{v}_{n,j}\sin(n\omega t), & n \in 3k, k \in N^+ \\ 0, & n \in 6k \pm 1, k \in N^+. \end{cases} \tag{26b}$$

For HWS, its harmonic phase $\phi_{n,j}$ is controllable, i.e.,

$$\begin{cases} v_{a,n,j} = \hat{v}_{n,j}\sin(n\omega t + \phi_{n,j}), & n \in 1,3,5,\dots \\ v_{b,n,j} = \hat{v}_{n,j}\sin(n\omega t - \frac{2\pi n}{3} + \phi_{n,j}), & n \in 1,3,5,\dots \\ v_{c,n,j} = \hat{v}_{n,j}\sin(n\omega t + \frac{2\pi n}{3} + \phi_{n,j}), & n \in 1,3,5,\dots \end{cases} \tag{27}$$

The harmonics in $v_{\mathrm{no},j}$ can be expressed

$$v_{\mathrm{no},j} = \begin{cases} \hat{v}_{n,j}\sin(n\omega t + \phi_{n,j}), & n \in 3k, k \in N^+ \\ 0, & n \in 6k \pm 1, k \in N^+. \end{cases} \tag{28}$$

Therefore, for the current injected to the power grid as (24), the triplen harmonics caused by the switching pulse are eliminated, and only the harmonics of $6k \pm 1$ orders are effective in the currents. Thus, the nth harmonic currents injected by jth power converter can be simplified as

$$i_{n,j} = \frac{\hat{v}_{n,j}\angle\varphi_{n,j}^*}{\hat{z}_{n,j}\angle 90}, \quad n \in 6k \pm 1, k \in N^+ \tag{29}$$

where $z_{n,j}$ is the equal independence of the jth filters under the nth harmonic, and $\varphi_{n,j}^*$ is the angle of the nth harmonic generated by the jth power converter, i.e.,

$$\varphi_{n,j}^* = \phi_{n,j}^* + \phi_{\mathrm{b},j}^* \tag{30}$$

where $\phi_{n,j}^* = \phi_{n,j} - \phi_{1,j}$ is the phase angle between the harmonics and the fundamental component of the switching signal (i.e., $\phi_{1,j}^* = 0$), and $\phi_{\mathrm{b},j}^*$ represents the phase deviation of the jth converter relative to the standard fundamental phase of the cluster. Typically, the fundamental phase of the 1th power converter is chosen as the reference phase in the cluster, i.e., $\phi_{\mathrm{b},1}^* = 0$.

According to Kirchhoff's law, the total current at the PCC can be obtained as follows:

$$i_{\mathrm{a,n,pcc}} = \sum_{j=1}^{N} \frac{\mathcal{K}_{n,j}}{n}\hat{v}_{n,j}\angle(\varphi_{n,j}^* - 90), \quad n \in 6k \pm 1 \tag{31}$$

where $\mathcal{K}_{n,j}$ is the system coefficient of the jth converter, i.e., $\mathcal{K}_j = \frac{n}{\hat{z}_{n,j}}$. N is the number of power converters in the cluster. Therefore, for the QaHWS-OPPs with the target of enhancing power quality in PCC, its optimization problem can be formulated as

$$\min_{\alpha_{i,j}} \sum_{n=5,7,11,\cdots} \left| \sum_{j=1}^{N} \frac{\mathcal{K}_{n,j}}{n} \hat{v}_{n,j} \angle(\varphi^*_{n,j} - 90) \right|^2 \tag{32a}$$

$$\text{s.t.} \quad \frac{4}{\pi} \sum_{i=1}^{d_j} \Delta u_{i,j} \cos(\alpha_{i,j}) = \mathcal{M}_j \tag{32b}$$

$$\left| \sum_{j=1}^{N} \frac{\mathcal{K}_{n,j}}{n} \hat{v}_{n,j} \angle(\varphi^*_{n,j} - 90) \right| \leq \mathcal{L}_n \tag{32c}$$

$$0 < \alpha_{1,\mathrm{j}} < \alpha_{2,\mathrm{j}} \ldots < \alpha_{d_j,j} < \frac{\pi}{2} \tag{32d}$$

$$\forall j \in \{1, 2, 3, \ldots, N\} \tag{32e}$$

where $\mathcal{M}_j$ is the desired modulation index of the jth power converter, $\mathcal{L}_n$ is the current harmonic limitations in PCC according to grid code [18], d_j is the pulse number of the jth power converter.

Accordingly, for GS-OPPs with HWS, the optimization problem is rebuilt as

$$\min_{\alpha_{i,j}} \sum_{n=5,7,11,\cdots} \left| \sum_{j=1}^{N} \frac{\mathcal{K}_{n,j}}{n} \hat{v}_{n,j} \angle(\varphi^*_{n,j} - 90) \right|^2 \tag{33a}$$

$$\text{s.t.} \quad \frac{2}{\pi} \sum_{i=1}^{2d_j} \Delta u_{i,j} \cos(\alpha_{i,j}) = \mathcal{M}_j \tag{33b}$$

$$\frac{2}{\pi} \sum_{i=1}^{2d_j} \Delta u_{i,j} \sin(\alpha_{i,j}) = 0 \tag{33c}$$

$$\left| \sum_{j=1}^{N} \frac{\mathcal{K}_{n,j}}{n} \hat{v}_{n,j} \angle(\varphi^*_{n,j} - 90) \right| \leq \mathcal{L}_n \tag{33d}$$

$$0 < \alpha_{1,\mathrm{j}} < \alpha_{2,\mathrm{j}} \ldots < \alpha_{2d_j,j} < \pi \tag{33e}$$

$$\forall j \in \{1, 2, 3, \ldots, N\}. \tag{33f}$$

B. Overall Optimization Problem

Minimizing THD at the PCC is an industry expectation, but individual converter power quality optimization is also important, especially for the deployment without a pulse-pattern-type controller [20], [21], [22]. Larger current harmonic ripples pose challenges to the control of individual converters (dynamics and stability problems caused by large time scale sampling filters). To achieve a balance between these two optimization objectives, the final optimization problem also accounts for individual converter optimization. The derivation of power quality optimization for a single converter can be found in Section III-D.

Therefore, for the GS-OPPs with QaHWS, the optimization problem considering the single power units is designed as

$$\min_{\alpha_{i,j}} \sum_{n=5,7,11,\cdots} \left| \sum_{j=1}^{N} \frac{\mathcal{K}_{n,j}}{n} \hat{v}_{n,j} \angle(\varphi^*_{n,j} - 90) \right|^2 \tag{34a}$$

$$+ \sum_{j=1}^{N} \rho_j \sum_{n=5,7,11,\ldots} \frac{1}{n^4} \left(\sum_{i=1}^{d_j} \Delta u_{i,j} \cos(n\alpha_{i,j}) \right)^2 \tag{34b}$$

$$\text{s.t.} \quad \frac{4}{\pi} \sum_{i=1}^{d_j} \Delta u_{i,j} \cos(\alpha_{i,j}) = \mathcal{M}_j \tag{34c}$$

$$\left| \sum_{j=1}^{N} \frac{\mathcal{K}_{n,j}}{n} \hat{v}_{n,j} \angle(\varphi^*_{n,j} - 90) \right| \leq \mathcal{L}_n \tag{34d}$$

$$0 < \alpha_{1,j} < \alpha_{2,j} \ldots < \alpha_{d_j,j} < \frac{\pi}{2} \tag{34e}$$

$$\forall j \in \{1, 2, 3, \ldots, N\}. \tag{34f}$$

For the GS-OPPs with HWS, the extra fundamental phase constraints are added, i.e.

$$\min_{\alpha_{i,j}} \sum_{n=5,7,11,\cdots} \left| \sum_{j=1}^{N} \frac{\mathcal{K}_{n,j}}{n} \hat{v}_{n,j} \angle(\varphi^*_{n,j} - 90) \right|^2 \tag{35a}$$

$$+ \sum_{j=1}^{N} \rho_j \sum_{n=5,7,11,\cdots} \left(\frac{\hat{u}_{n,j}}{n} \right)^2 \tag{35b}$$

$$\text{s.t.} \quad \frac{2}{\pi} \sum_{i=1}^{2d_j} \Delta u_{i,j} \cos(\alpha_{i,j}) = \mathcal{M}_j \tag{35c}$$

$$\frac{2}{\pi} \sum_{i=1}^{2d_j} \Delta u_{i,j} \sin(\alpha_{i,j}) = 0 \tag{35d}$$

$$\left| \sum_{j=1}^{N} \frac{\mathcal{K}_{n,j}}{n} \hat{v}_{n,j} \angle(\varphi^*_{n,j} - 90) \right| \leq \mathcal{L}_n \tag{35e}$$

$$0 < \alpha_{1,\mathrm{j}} < \alpha_{2,\mathrm{j}} \ldots < \alpha_{2d_j,j} < \pi \tag{35f}$$

$$\forall j \in \{1, 2, 3, \ldots, N\}. \tag{35g}$$

where ρ_j are the weighting factors of the jth power converter, used to balance the tradeoff between power quality optimization at the PCC and that of individual converters.

C. Implementation

GS-OPPs is a global-synchronized modulation algorithm that requires collecting the operating information of the power converter cluster and solving the look-up table (LUT) of pulse patterns for each single unit. Therefore, a global-synchronized computation unit (GSCU) is designed to implement it.

The deployment of GS-OPPs with a GSCU can be divided into four parts (see Fig. 6): 1) data collection, 2) pulse patterns

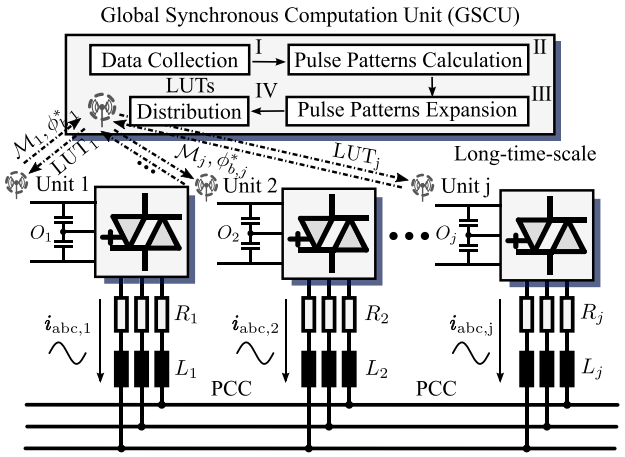

Fig. 6. Implementation of the proposed GS-OPPs with a GSCU.

calculation, 3) pulse patterns expansion for quasi-steady state, 4) LUTs distribution.

1) Data Collection (Step I): Under the quasi-steady state, the GSCU first collects the global information of each single power converter to form the optimization problem of GS-OPPs at the ideal operation point. The collected information includes: 1) the average modulation index $\mathcal{M}_j$, 2) dc bus voltage $V_{\mathrm{dc},j}$, 3) the phase deviation relative to the standard fundamental phase of the cluster $\phi^*_{\mathrm{b},j}$, 4) desired pulse number d_j, and 5) system impedance z_j. The system impedance z_j can be obtained through an online parameter identification algorithm (e.g., recursive least squares, digital twin [23], etc.).

2) Pulse Patterns Calculation (Step II): Based on the established optimization problems (34) and (35), the GS-OPPs at the ideal operating point can be calculated by several existing global optimization algorithms. Here, a Sequential Quadratic Programming (SQP) mathematical solver with multiple randomized initial guesses is employed to compute the pulse width sequence under ideal operating conditions.[2] Hereafter, the GS-OPPs $\boldsymbol{\alpha}^*_j$ at the operating point matching the collected data $(\mathcal{M}_j, V_{\mathrm{dc},j}, \phi^*_{\mathrm{b},j}, d_j, z_j)$ are obtained

$$\boldsymbol{\alpha}^*_j = [\alpha^*_{1,j}, \alpha^*_{2,j}, \cdots], \qquad \forall j \in \{1, 2, 3, \ldots, N\}. \tag{36}$$

3) Pulse Patterns Expansion for Quasi-Steady State (Step III): According to the previous step, the GS-OPPs for each power converter at the ideal operating point have been determined, i.e., $\boldsymbol{\alpha}^*_j$. Since the computation of GS-OPPs is not performed instantaneously, the OPP for each power converter are temporally expanded to ensure that the converter cluster maintains coordinated operation in a quasi-steady-state manner, i.e., obtaining the GS-OPPs at the adjacent operation points for a single power converter ($[\mathcal{M}^*_j - \mathcal{B}_j, \ldots, \mathcal{M}^*_j + \mathcal{B}_j]$). $\mathcal{B}_j$ is the modulation index fluctuation range of jth power converter in the system's quasi-steady state. During the computation, all converters except the extended unit are assumed to operate at their ideal operating points, with their pulse pattern LUTs already distributed.

[2] For more advanced solving algorithm of optimization problem, please refer to [19].

Algorithm 1: Pulse Patterns Expansion.

Input: $\boldsymbol{\alpha}^*_p$, $\mathcal{G}\angle\varphi_{\mathrm{con}}$
Output: LUTs for single units (pth unit for example)
1: Initialization $\boldsymbol{\alpha}^{\mathrm{opt}}_{\mathrm{last}} = \boldsymbol{\alpha}^*_p$ (Half Top LUT)
2: **for** $\mathcal{M}_p \in [\mathcal{M}^*_p, \ldots, \mathcal{M}^*_p + \mathcal{B}_p]$ **do**
3: Optimal inherit $\boldsymbol{\alpha}_{\mathrm{ini}} = \boldsymbol{\alpha}^{\mathrm{opt}}_{\mathrm{last}}$
4: Calculation $\boldsymbol{\alpha}^{\mathrm{opt}} =$ Solve (37) or (39)
5: Update $\boldsymbol{\alpha}^{\mathrm{opt}}_{\mathrm{last}} = \boldsymbol{\alpha}^{\mathrm{opt}}$
6: Collect the solution $\Rightarrow [\mathcal{M}_p, \alpha_1, \alpha_2, \ldots]$
7: **end for**
8: Initialization $\boldsymbol{\alpha}^{\mathrm{opt}}_{\mathrm{last}} = \boldsymbol{\alpha}^*_p$ (Half Bottom LUT)
9: **for** $\mathcal{M}_p \in [\mathcal{M}^*_p, \ldots, \mathcal{M}^*_p - \mathcal{B}_p]$ **do**
10: Optimal inherit $\boldsymbol{\alpha}_{\mathrm{ini}} = \boldsymbol{\alpha}^{\mathrm{opt}}_{\mathrm{last}}$
11: Calculation $\boldsymbol{\alpha}^{\mathrm{opt}} =$ Solve (37) or (39)
12: Update $\boldsymbol{\alpha}^{\mathrm{opt}}_{\mathrm{last}} = \boldsymbol{\alpha}^{\mathrm{opt}}$
13: Collect the solution $\Rightarrow [\mathcal{M}_p, \alpha_1, \alpha_2, \ldots]$
14: **end for**
15: **return** LUT for single unit $\Rightarrow [\mathcal{M}_p, \alpha_1, \alpha_2, \ldots], \ldots$

Here, take pth ($p \in \{1, 2, \ldots, N\}$) power converter as an example, the computational steps for extending GS-OPPs are as follows. Since the other converter units are assumed to operate at their ideal operating points with fixed pulse patterns, the optimization problem for extending GS-OPPs with QaHWS is reformulated as follows:

$$\min_{\alpha_{i,p}} \sum_{n=5,7,11,\cdots} \left| \frac{\mathcal{K}_{n,p}}{n} \hat{v}_{n,p} \angle(\varphi^*_{n,p} - 90) + \mathcal{G}\angle\varphi_{\mathrm{con}} \right|^2 \tag{37a}$$

$$+ \rho_p \sum_{n=5,7,11,\cdots} \frac{1}{n^4} \left(\sum_{i=1}^{d_p} \Delta u_{i,p} \cos(n\alpha_{i,p}) \right)^2 \tag{37b}$$

$$\text{s.t.} \quad \frac{4}{\pi} \sum_{i=1}^{d_p} \Delta u_{i,p} \cos(\alpha_{i,p}) = \mathcal{M}_p \tag{37c}$$

$$\left| \frac{\mathcal{K}_{n,p}}{n} \hat{v}_{n,p} \angle(\varphi^*_{n,p} - 90) + \mathcal{G}\angle\varphi_{\mathrm{con}} \right| \le \mathcal{L}_n \tag{37d}$$

$$0 < \alpha_{1,p} < \alpha_{2,p} \ldots < \alpha_{d_p,p} < \frac{\pi}{2} \tag{37e}$$

where

$$\mathcal{G}\angle\varphi_{\mathrm{con}} = \sum_{j \neq p}^{N} \frac{\mathcal{K}_{n,j}}{n} \hat{v}_{n,j} \angle(\varphi^*_{n,j} - 90). \tag{38}$$

Due to the previous assumptions, when j is unequal to p, the variables $\hat{v}_{n,j}$, $\varphi^*_{n,j}$ remain unchanged, making $\mathcal{G}\angle\varphi_{\mathrm{con}}$ a constant quantity during the optimization process. For GS-OPPs with HWS, the optimization problem for pulse pattern extension is expressed as

$$\min_{\alpha_{i,p}} \sum_{n=5,7,11,\cdots} \left| \frac{\mathcal{K}_{n,p}}{n} \hat{v}_{n,p} \angle(\varphi^*_{n,p} - 90) + \mathcal{G}\angle\varphi_{\mathrm{con}} \right|^2 \tag{39a}$$

$$+\rho_p \sum_{n=5,7,11,\cdots} \left(\frac{\hat{u}_{n,p}}{n}\right)^2 \tag{39b}$$

$$\text{s.t.} \quad \frac{2}{\pi}\sum_{i=1}^{2d_p} \Delta u_{i,p}\cos(\alpha_{i,p}) = \mathcal{M}_p \tag{39c}$$

$$\frac{2}{\pi}\sum_{i=1}^{2d_p} \Delta u_{i,p}\sin(\alpha_{i,p}) = 0 \tag{39d}$$

$$\left|\frac{\mathcal{K}_{n,p}}{n}\hat{v}_{n,p}\angle(\varphi^*_{n,p} - 90) + \mathcal{G}\angle\varphi_{\text{con}}\right| \le \mathcal{L}_n \tag{39e}$$

$$0 < \alpha_{1,p} < \alpha_{2,p} \ldots < \alpha_{2d_p,p} < \pi. \tag{39f}$$

A gradient descent-based numerical method is employed to solve the above problem. The optimal solution $\boldsymbol{\alpha}^{\text{opt}}_{\text{last}}$ obtained from the nearest computation is chosen as the initial value for iteration $\boldsymbol{\alpha}_{\text{ini}}$, to facilitate the convergence speed and also avoid the discontinuity in LUTs of GS-OPPs [24]. A pseudocode solving procedure is provided as Algorithm 1.

4) LUTs Distribution (Step IV): After the optimization and extension process, the GSCU distributes the computed LUTs to the corresponding power converters. These LUTs are used to update those originally stored in each individual converter unit.

Remark 1: Since GS-OPP is designed as a high-level optimization framework implemented through a centralized global synchronization unit, it does not interfere with the design of conventional distributed control schemes. For edge controllers, only local modulation LUT need to be adjusted accordingly. Moreover, the designed LUT extension mechanism enables the system to maintain effective coordination during the intervals of upper-layer optimization caused by computational constraints. However, ensuring reliable communication between the global synchronization unit and individual converters is essential. This can be achieved by leveraging existing upper-layer power dispatch communication channels. Furthermore, the adoption of established mesh communication frameworks—with built-in data encryption and multinode coordination—can also enhance the robustness of GS-OPP against network attacks and single-point communication failures.

V. Experimental Verification

In this section, the effectiveness of the proposed GS-OPPs and its performance comparison with the existing solutions are evaluated with a lab-constructed experimental test bench represented in Fig. 7. As depicted, the experimental setup consists of two power units, each of which is composed of a 3L-NPC) power converter and an L-type filter, representing distributed power generation systems. Detailed parameters are listed in Table I. During the test, two power units, supplied by independent dc sources Chroma 62060D-600, are working in grid-following mode and feeding power into the ac grid generated by Chroma 61830, through a unified interface. The test covers the comparison of several typical modulation techniques and the proposal, i.e., 1) classical carrier-based PWM (CBPWM), 2) global-synchronized carrier-based PWM (GS-CBPWM), 3) classical OPPs, and 4) the proposed GS-OPPs. Meanwhile, the impact of the weighting factors and stress tests under nonideal operating conditions are also evaluated. Detailed results are shown in Figs. 8– 20 and analyzed in the following.

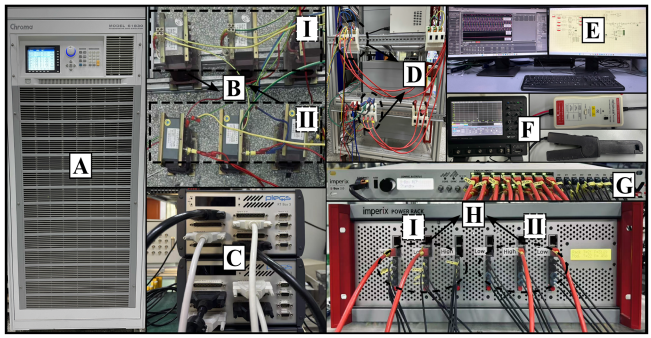

Fig. 7. The lab-constructed experimental test bench. (a) AC grid (Chroma 61830). (b) Power filters. (c) Controllers RT-BOX 3. (d) Current and voltage sensors. (e) Control desk and GSCU. (f) Oscilloscope and probes. (g) Controller B-BOX RCP. (h) Power units (3 L NPC power converters PEN8018, each of which is supplied by one independent DC Source Chroma 62060D-600).

TABLE I
System Setup in the Test

Description	Parameter	Value	Units
Grid frequency	f_{g}	50	[Hz]
Switching frequency	f_{sw}	250	[Hz]
DC Voltage	$V_{\text{dc},1,2}$	170	[V]
Grid Voltage	V_{ac}	50	[V]
Filter resistance	$R_{1,2}$	0.12	[Ω]
Filter inductance	$L_{1,2}$	10	[mH]

A. Performance Evaluation

In this section, the steady-state performance of the proposed GS-OPPs is first benchmarked against several existing modulation methods. To ensure the rigor of the evaluation, all systems operate under a proportional–integral (PI) control framework for grid current regulation. It is worth noting that both conventional OPPs and the proposed GS-OPPs are compatible with more advanced pulse pattern controllers, which can further enhance both transient and steady-state performance [20], [21], [22]. However, since this study focuses on the modulation stage, all control loops adopt the commonly used PI controller to ensure fairness in the comparison.

1) Classical Carrier-Based Modulation: First, the classical carrier-based modulation is implemented in the lab-constructed system to provide a reference for comparison. In the test, both converters operated in grid-following mode, with their reference set to 6 A. The switching frequency of each is set at 250 Hz to simulate the features in high power applications. Fig. 8(a) and (b) illustrates the currents in PCC and single units (phase a), respectively. As can be seen, limited by the finite switching frequency, considerable current/power ripples occur. The switching signals of each power converter are shown in Fig. 8(c) and (d), while the harmonic distortions in the sampling horizon (200 ms) are depicted in Fig. 8(e). Since classical CBPWM treats the modulation of each converter unit in isolation, the THD remains essentially the same at both the individual converter

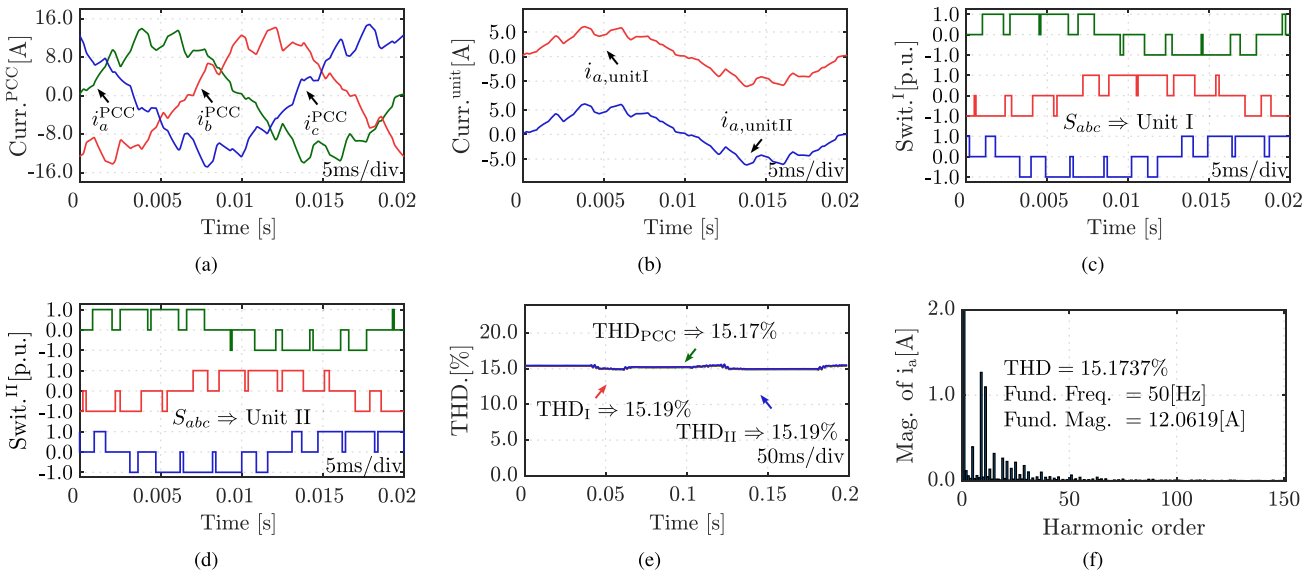

Fig. 8. [Experimental results] Classical carrier-based modulation. (a) Currents at PCC. (b) Current (phase a) in each power unit. (c) Pulse sequence of unit 1. (d) Pulse sequence of unit 2. (e) THDs. (f) FFT of the PCC currents.

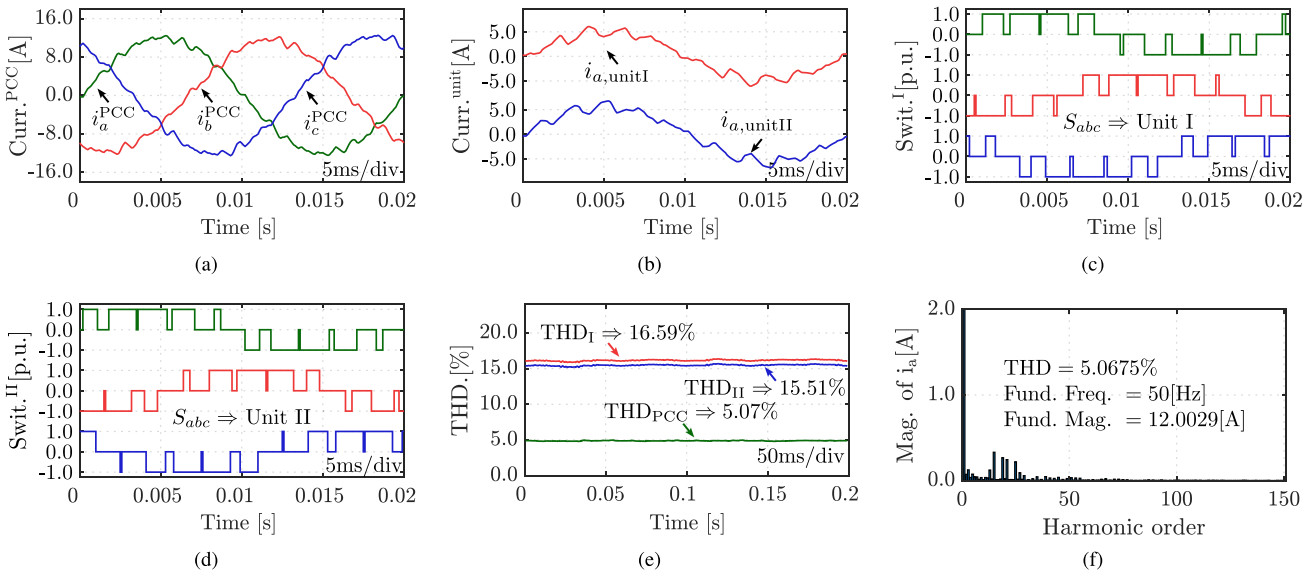

Fig. 9. [Experimental results] Global-synchronized carrier-based modulation. (a) Currents at PCC. (b) Current (phase a) in each power unit. (c) Pulse sequence of unit 1. (d) Pulse sequence of unit 2. (e) THDs. (f) FFT of the PCC currents.

level and the PCC. Fig. 8(f) presents the harmonic spectrum of the system currents at the PCC. Due to the characteristics of the carrier waveform, pronounced sideband harmonics appear around 250 ± 50 Hz. The average current THD at the system PCC reaches 15.17%, far exceeding the limits in grid codes.

2) Global-Synchronized Carrier-Based Modulation: To fully utilize the additional freedom provided by the converter cluster, a global-synchronized carrier-based modulation (GS-PWM) is proposed in [15]. The method solves an optimal carrier shifting in each power unit, thereby achieving a significant ripple reduction at PCC. The corresponding results of currents at PCC and individual power converters are shown in Fig. 9(a)–(b). Compared with traditional carrier-based modulation, the individual converter's current harmonic distortion remains nearly unchanged (slightly increased), while the THD at the PCC is significantly reduced. The switching pulse signals of the converters are depicted in Fig. 9(c) and (d). With optimized carrier shifting in each power converter, the pulse sequence in cluster systems has staggered switching instants, which is the inner reason for harmonic reduction at PCC. The THDs and the harmonic spectrum at the PCC are shown in Fig. 9(e) and (f), respectively. It can be observed that the characteristic harmonic at 250 ± 50 Hz has been significantly attenuated [compared to the

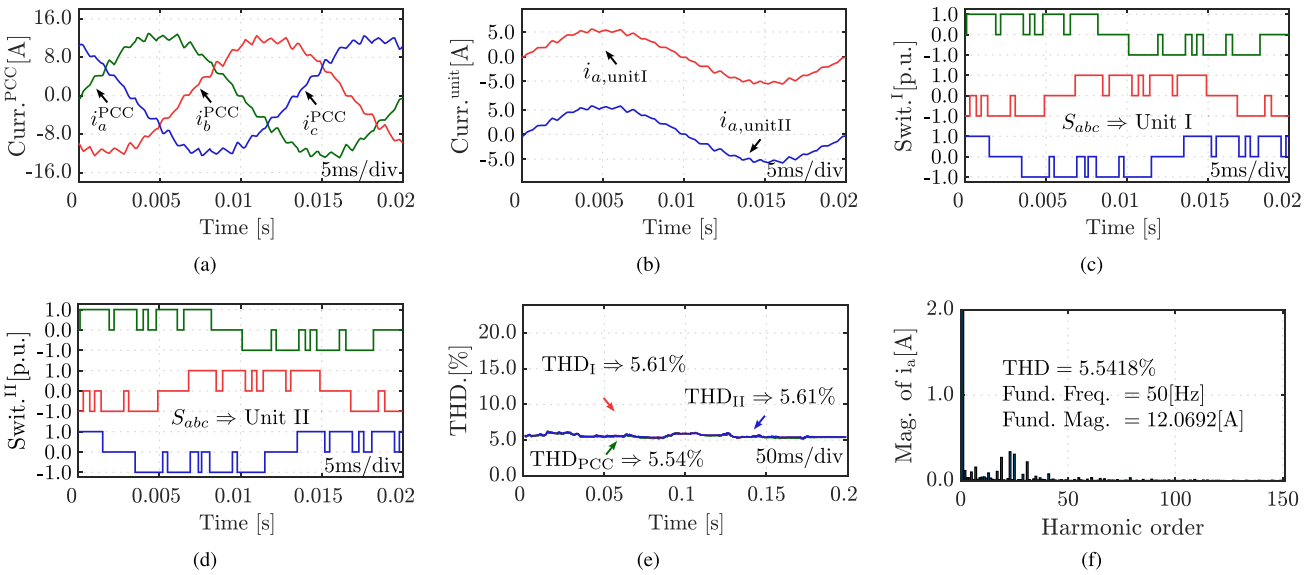

Fig. 10. [Experimental results] Classical optimal pulse patterns. (a) Currents at PCC. (b) Current (phase a) in each power unit. (c) Pulse sequence of unit 1. (d) Pulse sequence of unit 2. (e) THDs. (f) FFT of the PCC currents.

original one in Fig. 8(f)], and the THD has been reduced to 5%.

3) Classical OPPs: Here, the performance of classical OPPs is tested in the scenarios of converter clusters. The results are shown in Fig. 10. As depicted in Fig. 10(a) and (b), compared to the carrier-based modulation (see Fig. 8), OPP achieves a much higher power quality no matter in single units or PCC. The average current harmonic distortions are reduced from 15.2% to 5.6%, as shown in Fig. 10(e). However, the analysis perspective of classical OPPs is based on individual converters. Thus, it fails to fully utilize the pulse pattern coordination freedom offered by the converter cluster. As depicted in Fig. 10(c) and (d), with the same reference currents, the switching signals of the two converters are nearly identical. This results in the classical OPPs, when handling the optimization of a cluster system, even having a higher current THD at the PCC than the global-synchronized carrier modulation method, as shown in Fig. 10(f) (PCC: GS-CBPWM ⇒ 5.07%, OPPs ⇒ 5.54%).

4) Proposed GS-OPPs: In this test, the performance of the proposed GS-OPPs is benchmarked. First, the weighting coefficient for single-converter optimization is set to zero (i.e., $\rho_{1,2} = 0$) to evaluate the maximum improvement capability of GS-OPPs on the power quality at the PCC and its impact on each single power converter. The currents at the PCC and those of a single converter under GS-OPPs are shown in Fig. 11(a) and (b), respectively. It can be observed that the grid current at the PCC exhibits excellent power quality. However, due to the lack of consideration for the power quality of individual converters, the THD of each converter has actually increased. Although this has little impact from the grid's perspective (since the PCC serves as the actual grid interface), excessive harmonic content within individual power converters complicates the design of their internal control loops. Therefore, it is also necessary to suppress harmonics at the single-converter level. Fig. 11(e) and (f) illustrate the THD of each part within the converter cluster and the harmonic spectrum of the current at the PCC. As shown, the current harmonic distortion at the PCC is only 1.86%, representing a significant reduction compared to all previously tested modulation methods. To quantify the comparison, we define the power quality optimization degree $\mathcal{A}$ of GS-OPPs relative to other modulation methods as

$$\mathcal{A} = \frac{\mathrm{THD}_{\mathrm{ref}} - \mathrm{THD}_{\mathrm{GS-OPPs}}}{\mathrm{THD}_{\mathrm{ref}}} \times 100\% \tag{40}$$

where $\mathrm{THD}_{\mathrm{ref}}$ is the THD using the reference modulation method (classical OPPs or CBPWM, etc.), and $\mathrm{THD}_{\mathrm{GS-OPPs}}$ is the THD using the proposed GS-OPPs. The comparable results of GS-OPPs with $\rho_{1,2} = 0$ are collected in Table II. As shown, with the proposed GS-OPPs, the current power quality at the PCC of the converter cluster is significantly improved—achieving at least over 60% compared to all tested modulation methods. However, since the weighting factor for single-converter power quality optimization is set to zero, the power quality of individual grid-connected units deteriorates substantially.

TABLE II
OPTIMIZATION DEGREE OF GS-OPPS WITHOUT CONSIDERED OPTIMIZATION IN SINGLE UNITS $\rho_{1,2} = 0$

Index \ Type	Classical CBPWM	Classical GS-CBPWM	Classical OPPs
Current THD in PCC (avg.)	15.17%	5.067%	5.542%
Optimization Degree of GS-OPPs in PCC	87.74%	63.29%	66.44%

Subsequently, GS-OPPs with consideration of individual converter power quality optimization are also tested. In this case, the corresponding weight coefficients are set to 1 to tradeoff the optimization between PCC and single units, i.e., $\rho_{1,2} = 1$. The results are depicted in Fig. 12. As shown, the current THD at the PCC remains significantly lower compared to classical

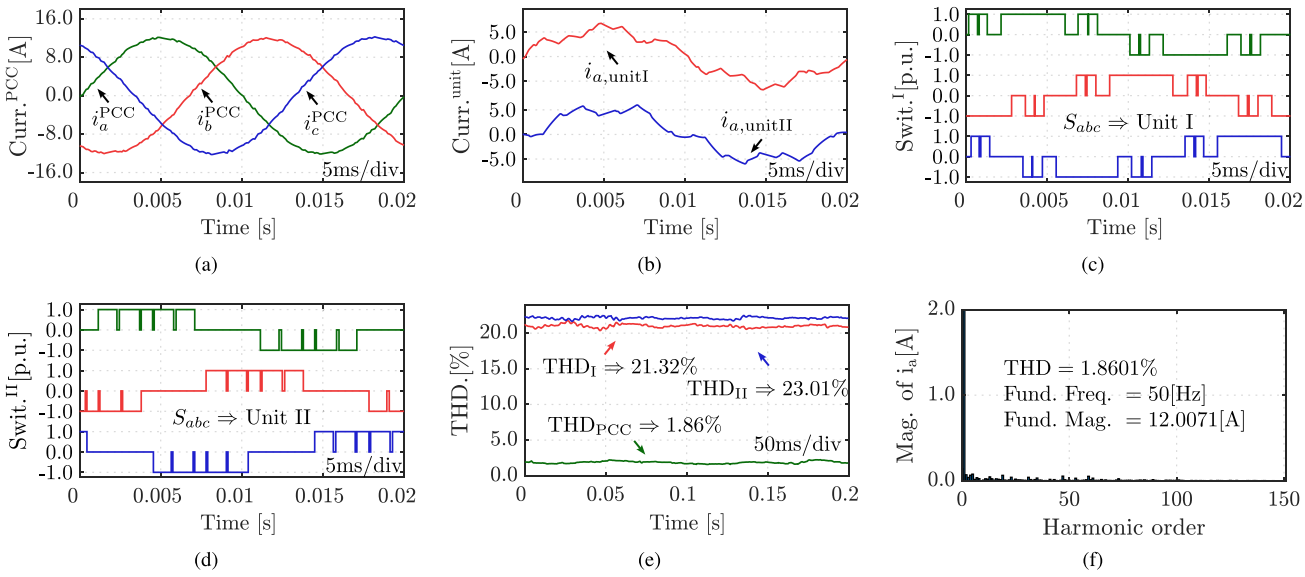

Fig. 11. [Experimental results] Proposed GS-OPPs with $\rho_{1,2} = 0$. (a) Currents at PCC. (b) Current (phase a) in each power unit. (c) Pulse sequence of unit 1. (d) Pulse sequence of unit 2. (e) THDs. (f) FFT of the PCC currents.

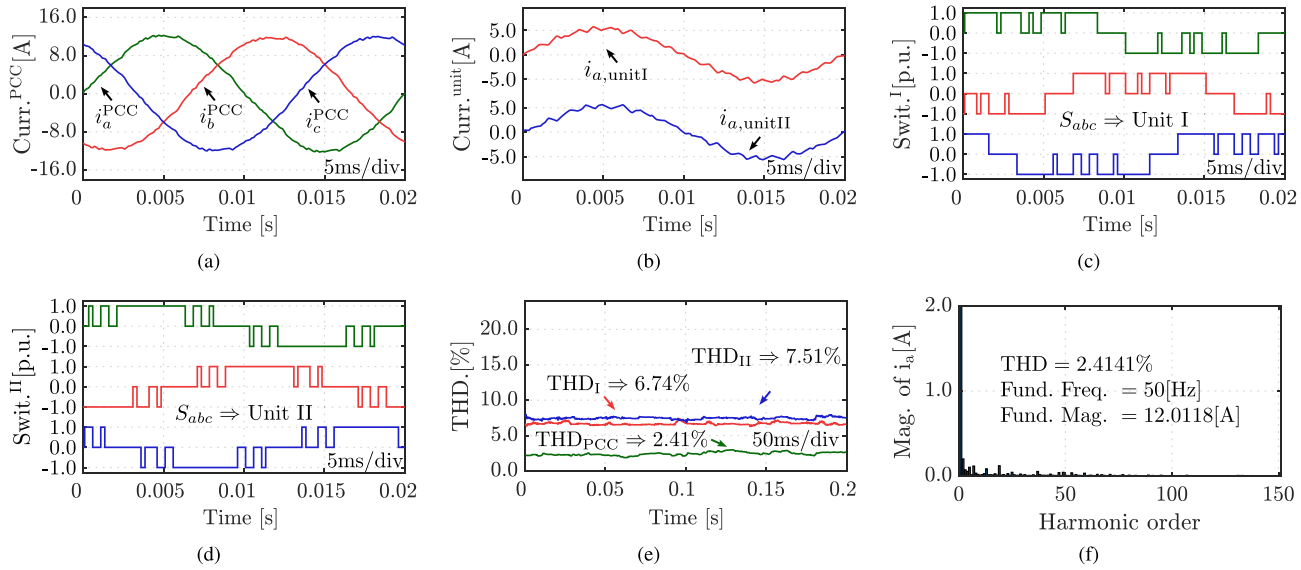

Fig. 12. [Experimental results] Proposed GS-OPPs with $\rho_{1,2} = 1$. (a) Currents at PCC. (b) Current (phase a) in each power unit. (c) Pulse sequence of unit I. (d) Pulse sequence of unit II. (e) THDs. (f) FFT of the PCC currents.

modulation methods like OPPs or GS-CBPWM. Moreover, by incorporating a tradeoff for individual converter power quality, the current THD of each converter is also substantially reduced. Compared to traditional carrier-based modulation, the THD of each individual converter is reduced from 15.17%to 7.51%. Note that the classical OPP focuses on optimizing the power quality of individual converters. As a result, the THD of individual units in the proposed GS-OPPs is slightly higher than that of the classical OPPs. However, from the perspective of the overall optimization goal for the converter cluster, GS-OPPs offer unparalleled advantages in optimizing the cluster's power quality. The current THD at the PCC is reduced from 5.54%to 2.41%.

Remark 2: In the above experimental tests, the steady performance of several classical modulation methods and the proposal are benchmarked in a converter cluster consisting of two power units. The results are further summarized in Table III. It can be observed that classical OPPs offer better power quality than classical carrier-based modulation under low switching frequencies. However, since the PCC serves as the actual grid interface of the converter cluster, optimizing its power quality is the ultimate goal. Classical OPPs, being designed from the viewpoint of individual converters, do not fully leverage the inherent advantages offered by clustered converter systems. Thereby, it has an even worse power quality than classical global-synchronized

TABLE III
THDs UNDER DIFFERENT MODULATION METHODS

Index / Type	Current THD in Unit I (avg.)	Current THD in Unit II (avg.)	Current THD in PCC (avg.)
Classical CBPWM	15.19%	15.19%	15.17%
Classical GS-CBPWM	16.59%	15.51%	5.07%
Classical OPPs	5.61%	5.61%	5.54%
GS-OPPs $\rho_{1,2} = 0$	21.32%	23.01%	1.86%
GS-OPPs $\rho_{1,2} = 1$	6.74%	7.51%	2.41%

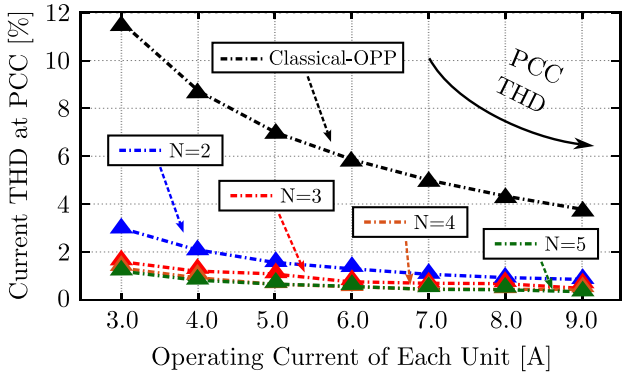

Fig. 13. [HIL results] Performance validation of GS-OPPs under multiple coordinated units.

CBPWM at the PCC. The proposed GS-OPPs overcome this limitation. In the above tests, the PCC current THD of the GS-OPPs is reduced by more than 60% compared to other modulation strategies.

B. Potential and Scalability Testing Across Multiple Units

In this section, the potential of GS-OPP is evaluated in coordination scenarios involving up to five converter units[3] with different symmetry configurations. Its performance across various power delivery levels is also demonstrated. Here, the RT Box 3 developed by PLECS was used to conduct tests involving more than two distributed generation units. To ensure consistency, all converter units and power circuit components were configured with identical parameters as shown in Table I.

1) Performance Validation With up to Five Coordinated Units: In this section, the performance of GS-OPPs is comprehensively evaluated under systems comprising two to five units. To ensure generality, each unit is tested under identical power references, with the coupling coefficient set to zero to highlight the maximum potential improvement. It can be observed that incorporating more coordinated units under the same operating conditions leads to enhanced cluster-level optimization (see Fig. 13). However, since the coordination among three to four units already achieves excellent THD reduction at the PCC, the additional benefit provided by the five-unit configuration becomes not obvious—especially when the unit power is relatively high. As shown in the figure, when the unit current reaches 9 A, the THD at the PCC is 0.349% for the five-unit system, compared to 0.410% for the four-unit system. Therefore, in renewable energy plants with a large number of power converters, deploying GS-OPP in parallel at the sub-unit level can be a viable strategy to achieve considerable THD optimization at the cluster level while maintaining computational efficiency (for detailed discussion of computational load, see Section V-D).

[3] The number of tested three-level NPC units is limited to five, constrained by the hardware capabilities of the hardware-in-the loop platform.

TABLE IV
TEST CONDITIONS (IN FIG. 14): POWER DISTRIBUTION AND UNIT CONFIGURATION

Test Index	Units	$I^*_{d,1}$	$I^*_{d,2}$	$I^*_{d,3}$	$I^*_{d,4}$	$I^*_{d,5}$	I^*_{PCC}
TI=1	N=2	5 A	5 A	-	-	-	10 A
TI=2	N=2	4 A	6 A	-	-	-	10 A
TI=3	N=3	4 A	5 A	6 A	-	-	15 A
TI=4	N=4	2 A	5 A	6 A	7 A	-	20 A
TI=5	N=5	2 A	3 A	4 A	6 A	10 A	25 A

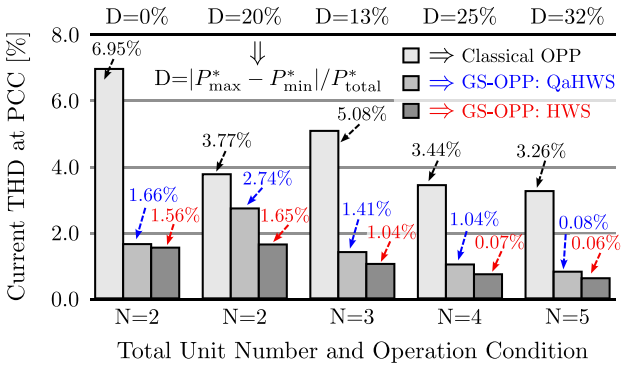

Fig. 14. [HIL results] Potential assessment of GS-OPPs with different symmetry under diverse power setups. From the left to right, the power configuration is set as Table IV.

2) Comprehensive Evaluation of GS-OPP With QaHWS and HWS: Here in this section, the tests aim to achieve two purposes: a) to evaluate the performance of GS-OPPs under various power distribution scenarios; and b) to explore its potential under different symmetry configurations. As the tests involve scenarios with varying power distributions across different units, the experimental configurations are summarized in Table IV in advance. The corresponding results are presented in Fig. 14. It can be observed that GS-OPP consistently outperforms the classical OPP in terms of steady-state performance across all test conditions. It is worth noting that GS-OPP with HWS exhibits greater optimization potential compared to QaHWS. This advantage becomes more pronounced in scenarios involving a small number of coordinated units with unequal power outputs. The primary reason lies in the phase-adjustability of harmonic components in HWS, which is absent in QaHWS. However, HWS entails a more complex mathematical formulation, resulting in an increased computational burden. Therefore, HWS is recommended when hardware resources are sufficient and the coordinated units are limited, whereas QaHWS is more suitable for a general choice due to its computational efficiency.

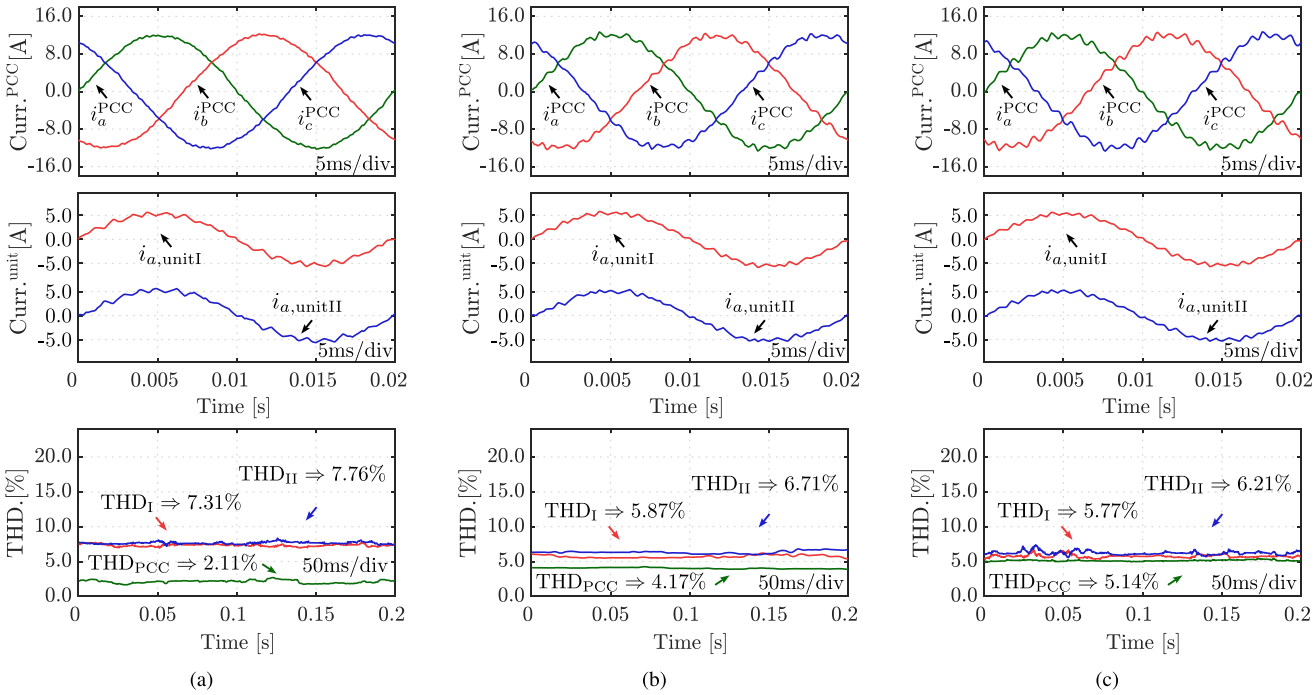

Fig. 15. [Experimental results] Performance trade off between PCC and single units. (a) GS-OPPs with the weighting factors set to 0.01, $\rho_{1,2} = 0.01$. (b) GS-OPPs with the weighting factors set to 5, $\rho_{1,2} = 5$. (c) GS-OPPs with the weighting factors set to 10, $\rho_{1,2} = 10$.

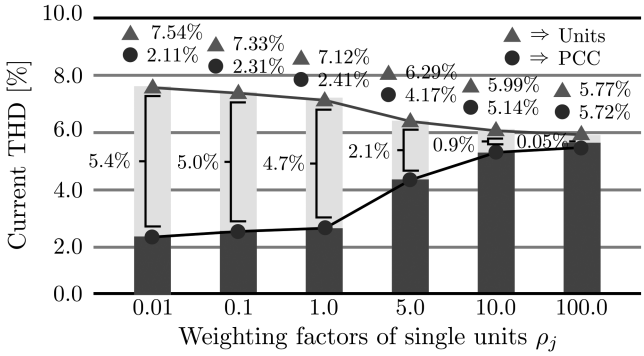

Fig. 16. [Experimental results] Impact of weighting factor ρ_j in GS-OPPs.

C. Tradeoff Between PCC and Single Units

In this section, the effects of different weighting coefficients are evaluated to explore the optimization tradeoff between PCC and single units. The results are shown in Fig. 15. In the test, the weighting factors are set as $\rho_{1,2} = 0.01$, $\rho_{1,2} = 5$, and $\rho_{1,2} = 10$, respectively. As can be seen, the GS-OPPs with smaller single-converter weighting coefficients achieve better power quality at the PCC, but at the cost of increased THD in individual converters. As compared to Fig. 15(a) and (c), the GS-OPP with $\rho_{1,2} = 0.01$ achieves a lower current THD at the PCC, i.e., 2.11%, lower than that of the GS-OPP with $\rho_{1,2} = 10$ by 5.14%. In contrast, the average current THD of individual converters increases to 7.54%, compared to 5.99% for $\rho_{1,2} = 10$. Fig. 16 presents more focused test data. As the weight coefficient ρ_j for individual converters increases, the PCC point optimization capability of GS-OPPs gradually decreases, while the power quality of the individual converters improves. Eventually, the performance converges toward that of the classical OPPs. Conversely, as the weight coefficient for the individual converters decreases, the optimization of the PCC point by GS-OPPs increases. However, this comes at the cost of a certain deterioration in the power quality of the individual converters. These results indicate that the influence of weighting coefficients on GS-OPP performance is both predictable and tunable. Their selection should be treated as a flexible design parameter, tailored to meet specific engineering objectives and tradeoffs.

D. Computation Load and Optimality

From a mathematical perspective, GS-OPP essentially constitutes a highly nonlinear upper-layer optimization problem. As such, there exists an inherent tradeoff between computational burden and solution optimality. Increasing the number of initial guesses improves the distribution of solution optimality, but at the cost of longer computation time. Here, we evaluated the solution optimality distribution and computation time of the two-unit GS-OPP with QaHWS under different population sizes. The corresponding results are presented in Fig. 17. For each test condition, 100 trials were conducted, and the results were statistically summarized in the form of a violin plot. It can be observed that, as the population size increases, the cost function tends to converge toward lower value regions, indicating improved solution quality. However, this improvement comes at

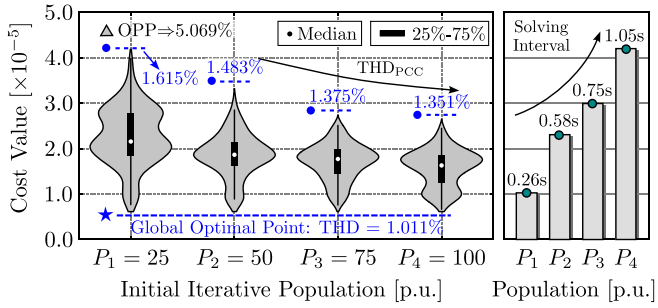

Fig. 17. [HIL results] Tradeoff between computational load and optimality.

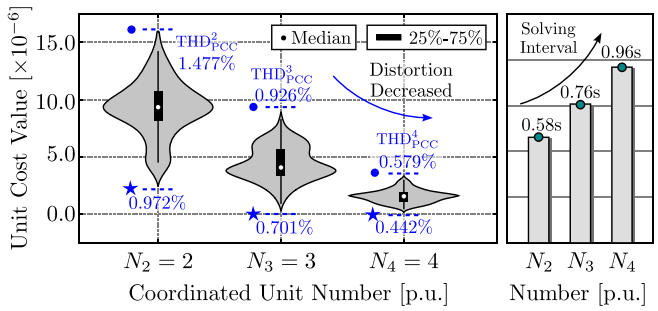

Fig. 18. [HIL results] Computation load and optimality in multiunit GS-OPP.

the expense of increased computational burden. Nevertheless, even when the optimization converges to a local optimum, the resulting power quality remains significantly better than that achieved by the conventional scheme.

Using a population size of 50 as the baseline, we further evaluated the computation time and solution optimality of GS-OPP with 2, 3, 4 converter units. To enable an intuitive comparison of the convergence points under different unit counts, the unit cost value is defined as $J_{\text{avr}} = J/N$. As shown in Fig. 18, even in the worst-case scenario—i.e., with the highest cost value—GS-OPP delivers significantly better power quality at the PCC compared to the conventional scheme. Notably, the computation time for the four-unit case is approximately 1s, while that for the two-unit case is only 0.58 s. With the LUT-based extension mechanism in the upper-layer optimization framework, the computation time is already sufficiently enough for GS-OPP.

Remark 3: The computational burden is indeed a challenging issue, particularly as the number of coordinated converter units increases. However, as demonstrated in Figs. 13 and 18, coordination among just two to four units already yields remarkable results, with a significant reduction in harmonic distortion compared to conventional methods. This observation suggests that, in large-scale energy plants with a high number of converter units, a group-divided strategy can be adopted—where each GS-OPP instance coordinates only a subset of units within a dedicated thread. In this way, GS-OPP can deliver highly effective results even in high-power systems with a large number of converters, while keeping the computational complexity manageable. Of course, coordinating more units generally yields

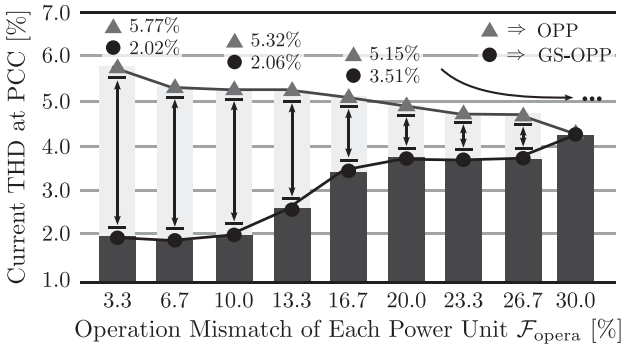

Fig. 19. [Experimental results] Stress test of operation mismatch under optimization interval.

better results, and the optimal grouping should be determined based on the available processing capabilities.

E. Stress Testing Under Non-Ideal Operating Conditions

In this section, the coordination performance of GS-OPP under nonideal conditions is evaluated. Two scenarios are considered: 1) coordination effectiveness under operating condition mismatches during upper-layer optimization intervals; and 2) coordination performance when mismatches occur in the optimized link circuit parameters.

1) Operation Mismatch Under Optimization Intervals: To evaluate the limit of GS-OPP's coordination performance under extended optimization intervals, stress tests are conducted under conditions where a significant mismatch is deliberately introduced between the control execution and the computed operating state. Here, we test the most adverse case for GS-OPP: a two-unit scenario with power mismatch in opposite directions—one unit with a positive mismatch and the other with a negative mismatch. This condition induces the largest possible deviation in both phase angle and modulation index. The experimental results are collected in Fig. 19. The horizontal axis in the figure represents unit nonuniformity, which is defined as

$$\mathcal{F}_{\text{opera}} = \frac{|P^*_{\text{max}} - P^*_{\text{min}}|}{P^*_{\text{avr}}} \tag{41}$$

It can be observed that the proposed GS-OPP maintains coordination performance across a wide range of operating mismatches. However, it is undeniable that when the mismatch reaches 30%, GS-OPP becomes less effective than the conventional OPP. Therefore, it is recommended that local controllers also retain a classical OPP implementation to allow fallback operation when significant deviation is detected. However, it is worth noting that such a 30% mismatch only occurs under extreme conditions, given the characteristic of MW application and optimization interval in practice.

2) Impact of Parameter Mismatch: In this section, the performance of GS-OPPs under parameter mismatches is evaluated. Here, we first define the degree of system parameter mismatch $\mathcal{F}_{\text{para}}$. Taking the system with two power converters as an example, if the system parameters deviate in the same direction and with equal magnitude, the constructed GS-OPPs remain

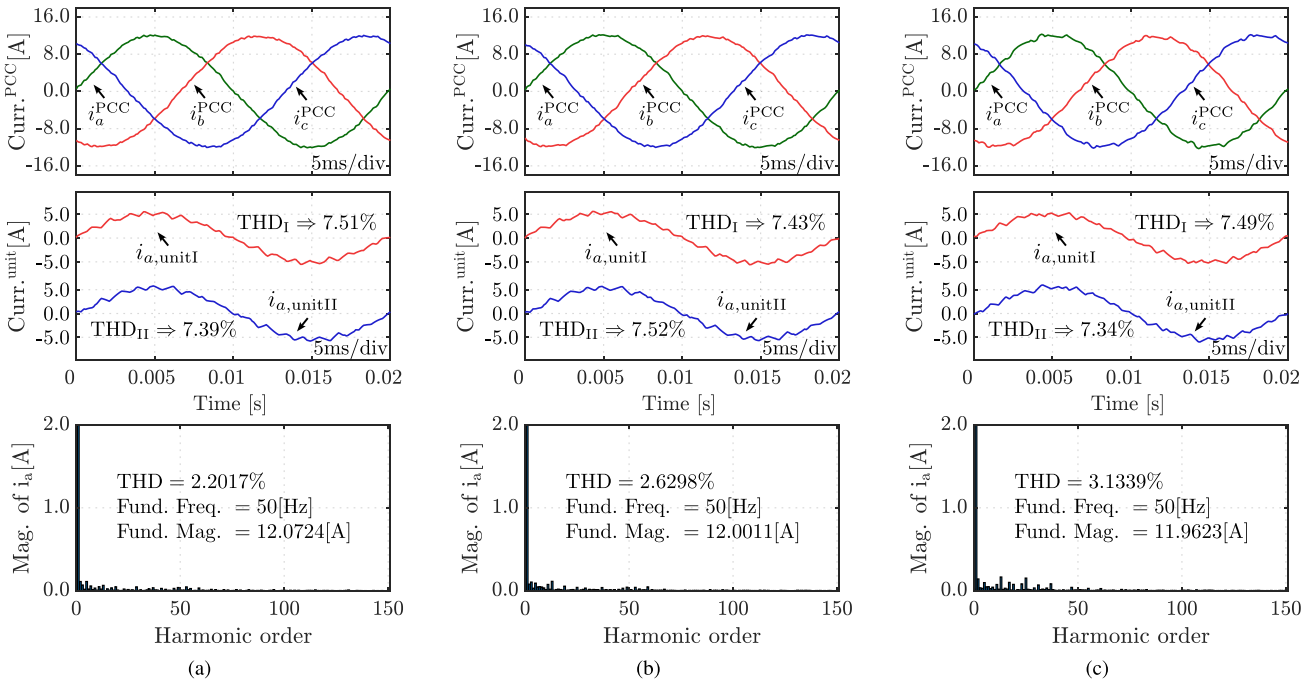

Fig. 20. [Experimental results] Performance of GS-OPPs with mismatched circuit parameters. (a) GS-OPPs with 5% parameter mismatch, $\mathcal{F}_{\text{para}} = 5\%$. (b) GS-OPPs with 20% parameter mismatch, $\mathcal{F}_{\text{para}} = 20\%$. (c) GS-OPPs with 40% parameter mismatch, $\mathcal{F}_{\text{para}} = 40\%$.

unaffected. As shown in (34) and (35), such deviation merely alters the relative weights between PCC-level and single-unit optimizations. Only when the inductance parameters of the two converters shift in opposite directions does the impact on GS-OPPs become most pronounced. Therefore, the parameter mismatch level is defined as follows:

$$\mathcal{F}_{\text{para}} = \left| \frac{\hat{z}^*_{n,1} - \hat{z}_{n,1}}{\hat{z}^*_{n,1}} - \frac{\hat{z}^*_{n,2} - \hat{z}_{n,2}}{\hat{z}^*_{n,2}} \right| \times 100\% \qquad (42)$$

where $\hat{z}_{n,1}$ and $\hat{z}_{n,2}$ represent the circuit parameters used in the GS-OPPs calculation, while $\hat{z}^*_{n,1}$ and $\hat{z}^*_{n,2}$ are the actual circuit parameters of the power circuit. In this test, we set the parameter mismatch degree of GS-OPPs to 5%, 20%, and 40%, with the system's single-unit weight coefficient set to 0.01. Therefore, the test results with no parameter mismatch can be found in Fig. 15(a). In the test process, the most impactful form of reverse mismatch was chosen, where for a 40% mismatch, the parameters of Unit 1 and Unit 2 deviate by 20% in opposite directions during the calculation. The results are shown in Fig. 20. Fig. 20(a) shows the performance of GS-OPPs with a 5% parameter mismatch. From top to bottom, the figure presents the currents at the PCC, the currents of single converters, and the harmonic spectrum at the PCC. As shown, compared to the case with no parameter mismatch in Fig. 15(a), the optimization of THD at the PCC is largely preserved, with only a slight decrease. Fig. 20(b) and (c) presents the experimental test results of GS-OPPs with 20% and 40% parameter mismatches, respectively. As depicted, the optimization of single-unit power quality is almost unaffected. However, when significant parameter mismatches occur, the optimization of the PCC deteriorates. At a 40% parameter mismatch, the THD at the PCC is degraded to 3.13%. Nevertheless, even in this case, the power quality at the PCC remains significantly higher than that of classical OPPs and GS-CBPWM. Moreover, such mismatches can be easily addressed through existing parameter identification algorithms [23], which can restore the system's performance.

VI. Conclusion

Clustered distribution of converter-based renewable power plants, offering higher reliability, lower power delivery fluctuations, and reduced maintenance costs, has become the dominant form of modern renewable energy generation. The form of clustering increases the control freedom for high-dimensional optimization and leads to a potential to further improve system performance. In this work, we propose a GS-OPP technique. Through establishing the harmonic models with multiple power unit interfaces and forming a global optimization problem in sequence distribution, the proposal significantly decreases the distortion of the grid-tied current at no addition in switching frequency or power filters. Experimental data confirm its effectiveness. The key features are as follows:

1) It offers more flexible harmonic management for the renewable plant with clustered converter configuration.
2) It achieves extreme power quality at PCC points, with extreme THD reduction, even with a few coordinated units.
3) It possesses strong versatility and can be easily applied to systems with PCC points, e.g., renewable energy generation plants, parallel power converter systems, etc.

Future work will focus on the efficiency of the calculations.

REFERENCES

[1] F. Blaabjerg and K. Ma, "Future on power electronics for wind turbine systems," *IEEE J. Emerg. Sel. Topics Power Electron.*, vol. 1, no. 3, pp. 139–152, Sep. 2013.

[2] A. Q. Huang, "Power semiconductor devices for smart grid and renewable energy systems," *Proc. IEEE*, vol. 105, no. 11, pp. 2019–2047, Nov. 2017.

[3] S. R. Bowes, "New sinusoidal pulsewidth-modulated invertor," *Proc. Inst. Elect. Eng.*, vol. 122, no. 11, pp. 1279–1285, 1975.

[4] N. Celanovic and D. Boroyevich, "A fast space-vector modulation algorithm for multilevel three-phase converters," *IEEE Trans. Ind. Appl.*, vol. 37, no. 2, pp. 637–641, Mar./Apr. 2001.

[5] P. N. Enjeti, P. D. Ziogas, and J. F. Lindsay, "Programmed pwm techniques to eliminate harmonics: A critical evaluation," *IEEE Trans. Ind. Appl.*, vol. 26, no. 2, pp. 302–316, Mar./Apr. 1990.

[6] F. G. Turnbull, "Selected harmonic reduction in static D-C — A-C inverters," *IEEE Trans. Commun. Electron.*, vol. 83, no. 73, pp. 374–378, Jul. 1964.

[7] M. Wu, C. Xue, Y. W. Li, and K. Yang, "A generalized selective harmonic elimination pwm formulation with common-mode voltage reduction ability for multilevel converters," *IEEE Trans. Power Electron.*, vol. 36, no. 9, pp. 10753–10765, Sep. 2021.

[8] M. Wu, H. Tian, Y. W. Li, G. Konstantinou, and K. Yang, "A composite selective harmonic elimination model predictive control for seven-level hybrid-clamped inverters with optimal switching patterns," *IEEE Trans. Power Electron.*, vol. 36, no. 1, pp. 274–284, Jan. 2021.

[9] R. P. Aguilera et al., "Selective harmonic elimination model predictive control for multilevel power converters," *IEEE Trans. Power Electron.*, vol. 32, no. 3, pp. 2416–2426, Mar. 2017.

[10] G. S. Buja and G. B. Indri, "Optimal pulsewidth modulation for feeding AC motors," *IEEE Trans. Ind. Appl.*, vol. IA-13, no. 1, pp. 38–44, Jan. 1977.

[11] I. Koukoula, P. Karamanakos, and T. Geyer, "Optimal pulse width modulation of three-level converters with reduced common-mode voltage," *IEEE Trans. Ind. Appl.*, vol. 60, no. 3, pp. 4062–4075, May/Jun. 2024.

[12] T. Geyer, P. Karamanakos, and I. Koukoula, "Optimized pulse patterns with bounded semiconductor losses," *IEEE Trans. Power Electron.*, vol. 39, no. 3, pp. 3233–3243, Mar. 2024.

[13] T. Dorfling and T. Geyer, "Thermally constrained optimized pulse patterns for medium-voltage neutral-point-clamped converters," *IEEE Trans. Power Electron.*, vol. 39, no. 10, pp. 13160–13176, Oct. 2024.

[14] A. Birth, T. Geyer, H. d. T. Mouton, and M. Dorfling, "Generalized three-level optimal pulse patterns with lower harmonic distortion," *IEEE Trans. Power Electron.*, vol. 35, no. 6, pp. 5741–5752, Jun. 2020.

[15] T. Xu and F. Gao, "Global synchronous pulse width modulation of distributed inverters," *IEEE Trans. Power Electron.*, vol. 31, no. 9, pp. 6237–6253, Sep. 2016.

[16] ABB, "Industrial drive,acs6080," May 2021. [Online]. Available: https://new.abb.com/drives/medium-voltage-ac-drives/acs6080

[17] HOPEWIND, "3300v full-power converter," Accessed: Oct. 9, 2025. [Online]. Available: https://www.hopewind.com/products-info/standard-cabinet-type-medium-voltage-wind-power-converter

[18] *IEEE recommended practices and requirements for harmonic control in electrical power systems*, IEEE Std 519-1992, pp. 1–112, 1993.

[19] Z. Zhang, G. Chen, and D. Xu, "Harmonic programmed modulation for high-power medium voltage energy conversion: Formulation, solving approach, and implementation," *IEEE Trans. Power Electron.*, vol. 40, no. 6, pp. 7872–7892, Jun. 2025.

[20] M. A. W. Begh, P. Karamanakos, and T. Geyer, "Gradient-based predictive pulse pattern control of medium-voltage drives—Part I: Control, concept, and analysis," *IEEE Trans. Power Electron.*, vol. 37, no. 12, pp. 14222–14236, Dec. 2022.

[21] T. Dorfling, H. d. T. Mouton, and T. Geyer, "Generalized model predictive pulse pattern control based on small-signal modeling—Part 1: Algorithm," *IEEE Trans. Power Electron.*, vol. 37, no. 9, pp. 10476–10487, Sep. 2022.

[22] T. Geyer, N. Oikonomou, G. Papafotiou, and F. D. Kieferndorf, "Model predictive pulse pattern control," *IEEE Trans. Ind. Appl.*, vol. 48, no. 2, pp. 663–676, Mar./Apr. 2012.

[23] W. Song, Z. Zhang, S. Zhang, C. Ma, and J. Li, "Digital twin modeling and multiparameter monitoring schemes of three-level ANPC inverters," *IEEE Trans. Power Electron.*, vol. 39, no. 12, pp. 16596–16608, Dec. 2024.

[24] A. K. Rathore, J. Holtz, and T. Boller, "Synchronous optimal pulsewidth modulation for low-switching-frequency control of medium-voltage multilevel inverters," *IEEE Trans. Ind. Electron.*, vol. 57, no. 7, pp. 2374–2381, Jul. 2010.

Guangze Chen (Student Member, IEEE) was born in Shandong, China, in 2002. He received the B.Sc. degree in electrical engineering in 2024 from Shandong University, Shandong, China, where he is currently working toward the Ph.D. degree in electrical engineering with the Laboratory for More Power Electronic Energy Systems, School of Electrical Engineering.

His research interests include modulation and control for high power energy conversion.

Zhenbin Zhang (Senior Member, IEEE) was born in Shandong, China, in 1984. He received the Ph.D. (*summa cum laude*) degree in electrical and energy engineering from the Technical University of Munich, Munich, Germany, in 2016.

He was a Postdoctoral in electrical and energy engineering with the Technical University of Munich, Munich, Germany. Since 2017, he has been a Full Professor with Shandong University, Jinan, China, where he is currently the Director for both the Laboratory of More Power Electronics Energy Systems and the Institute of Sustainable Energy and Smart Grids. His research interests include power electronics and electrical drives, and sustainable energy systems.

Dr. Zhang was the recipient of the VDE Award-2017 in Suedbayern, Germany, and is an Associate Editor for IEEE TRANSACTIONS ON POWER ELECTRONICS. He is currently an IET Fellow Member and IET Chartered Engineer.